

Supporting Information
for
Orientation of BINOL Grafted onto TiO₂

Christian A. Contreras¹, Ryan A. Hackler¹, Justin M. Notestein^{2*}, and Peter C. Stair^{1*}

¹ Department of Chemistry, Northwestern University, 2145 Sheridan Rd, Evanston, IL USA
60208

² Department of Chemical and Biological Engineering, Northwestern University, 2145 Sheridan
Road, Evanston, IL USA 60208

*corresponding author emails: j-notestein@northwestern.edu, pstair@northwestern.edu

Table of Contents

Figure S1. Comparison of solution absorption spectra of BINOL before and after grafting, and of the wash solution.

Figure S2. DRUV spectra of 1, 4, and 8 ALD cycles of TTIP onto BINOL-free Al₂O₃ to grow Xc-TiO₂-Al₂O₃. Spectra are referenced against bare Al₂O₃.

Figure S3. Compiled mass loss profiles of BINOLates grafted onto TiO₂.

Figure S4. Normalized DRIFT spectra of BINOLates and grafted BINOLates between 1100-1700 cm⁻¹

Table S1. Observed IR frequencies for BINOLates and BINOLates-TiO₂

Figure S5. Normalized DRIFT spectra of BINOLates and grafted BINOLates between 2600-3800 cm⁻¹

Figure S6. DRUV spectra of supported BINOLate-TiO₂ species. Spectra normalized by unmodified TiO₂ powder

Figure S7. Surface enhanced Raman spectra of BINOL-Al₂O₃ modified by 5, 10, and 15 cycles of Al₂O₃ by ALD.

Table S2. Observed SERS frequencies (ν , in cm⁻¹) of ALD TiO₂ deposited on BINOL-Al₂O₃-AgFON for 5, 10, and 15 cycles of TiO₂

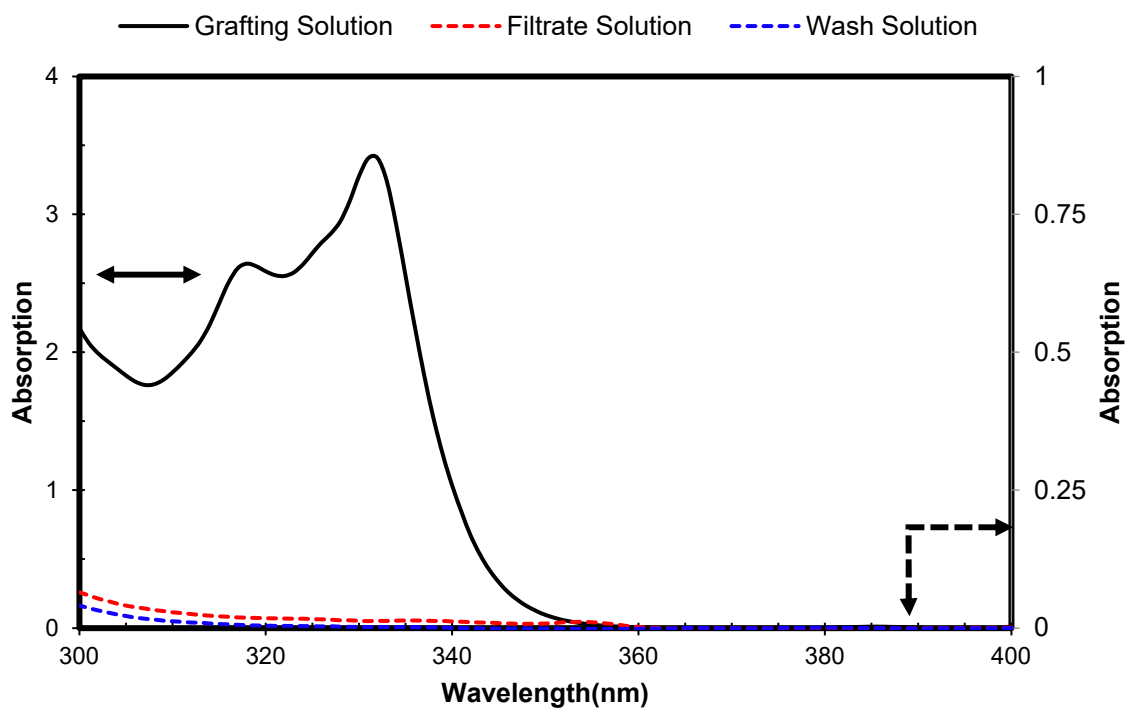


Figure S1. Comparison of solution absorption spectra of BINOL before and after grafting, and of the wash solution.

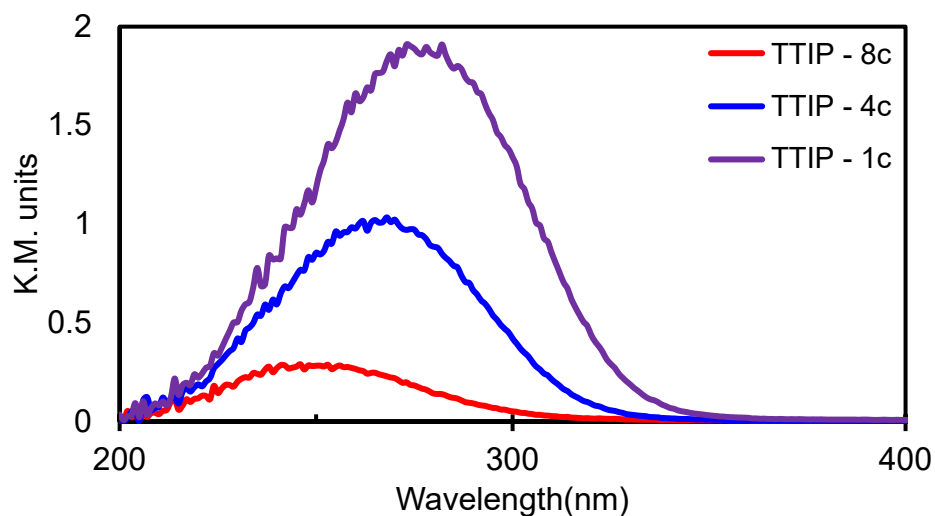


Figure S2. DRUV spectra of 1, 4, and 8 ALD cycles of TTIP onto BINOL-free Al_2O_3 to grow Xc- TiO_2 - Al_2O_3 . Spectra are referenced against bare Al_2O_3 .

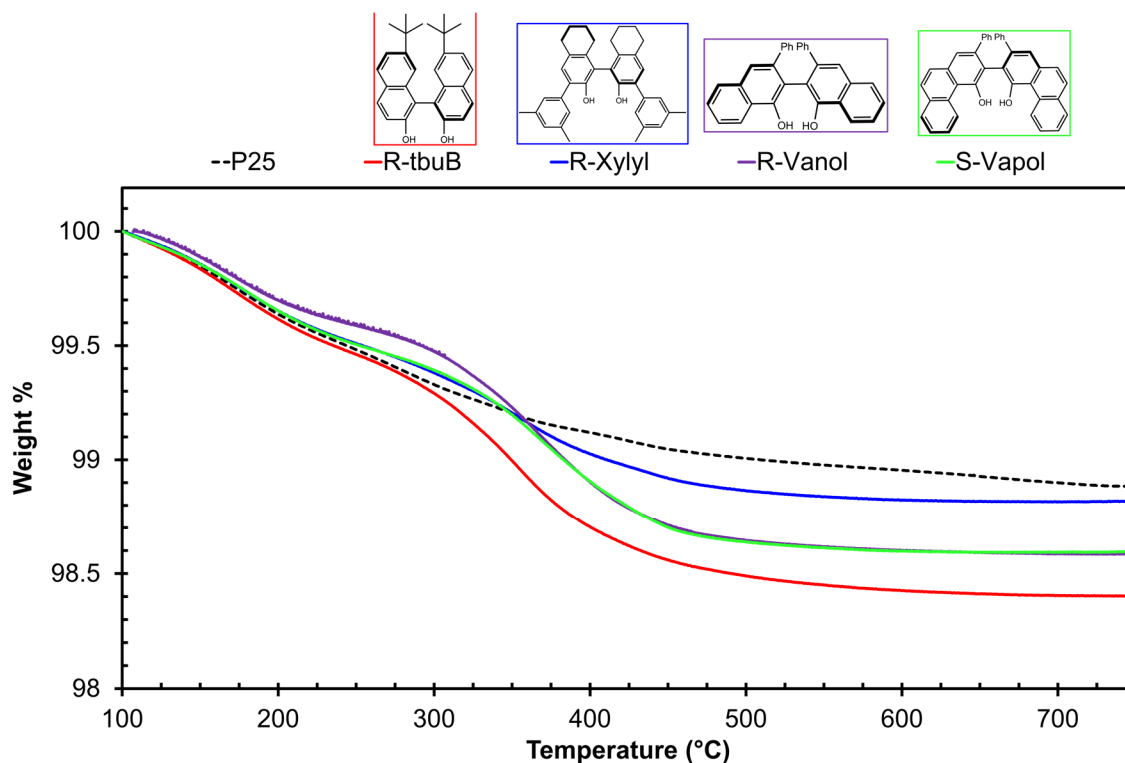


Figure S3. Compiled mass loss profiles of BINOLates grafted onto TiO₂. All materials were synthesized with an intended surface density of 0.14 BINOLate/nm². Mass loss in dry synthetic air was assumed to be due to complete combustion of the BINOLate between 300° and 600°C. Relative to the mass loss of unfunctionalized TiO₂ due to surface hydroxyl condensation, the loading of the individual BINOLates were 0.13-0.14 BINOLate/nm² for 6,6'-di-tertbutyl-BINOL, VANOL, and VAPOL. 3,3'-xylyl-BINOL grafted to only 0.05 BINOLate/nm².

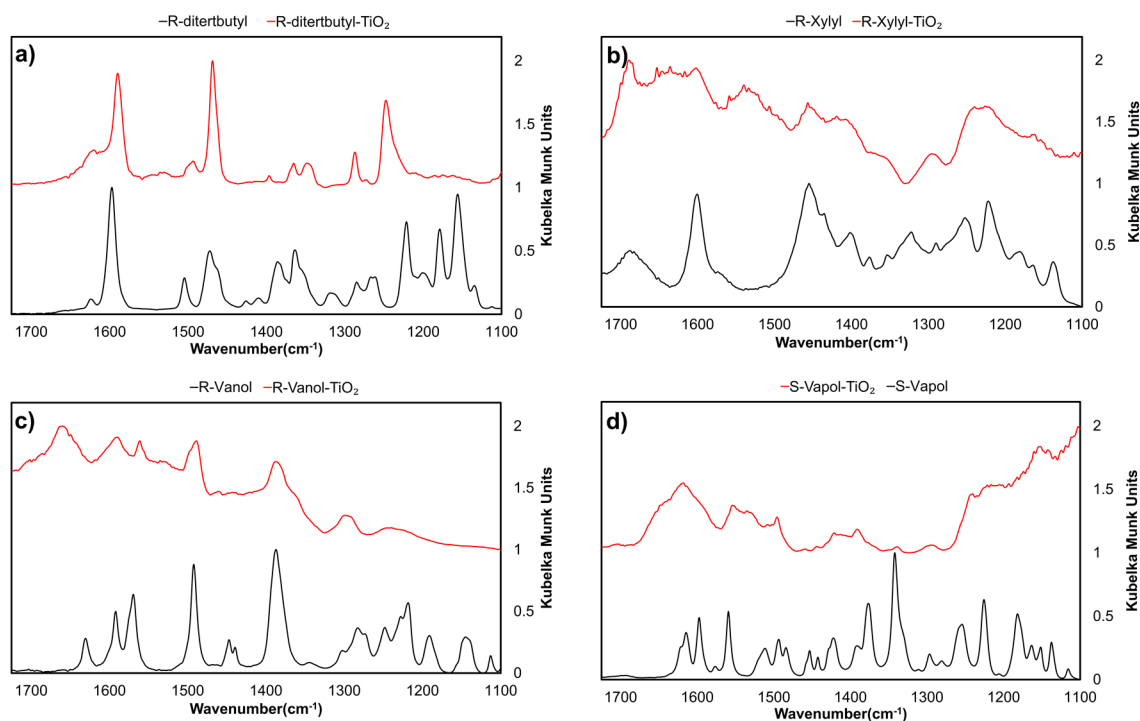


Figure S4. Normalized DRIFT spectra of BINOLates and grafted BINOLates (BINOLate-TiO₂) between 1100 and 1700 cm⁻¹ a) R-6,6'-di-tertbutyl-BINOL b) R-3,3'-xylyl-BINOL, c) R-VANOL, d) S-VAPOL. Spectra are stacked and normalized by their largest intensity for ease of comparison.

Table S1. Observed IR frequencies (ν in cm⁻¹) and their preliminary assignments for BINOLates and BINOLates-TiO₂

6,6'-di-tertbutyl-BINOL		3,3'-xylyl-BINOL		VANOL		VAPOL		Assignment
mol	grafted	mol	grafted	mol	grafted	mol	grafted	
1597	1590	1600	1600	1630	1640	1613	1618	vCC, vCO, vCC
1504	1492			1492	1487 (br)	1511	1495	vCO, δ C-H
1385	1363			1387	1381 (br)	1376	-	vCO, vCC
1284	1287	1289	1290 (br)	1281	1290			vCC, vCO, δ O-H

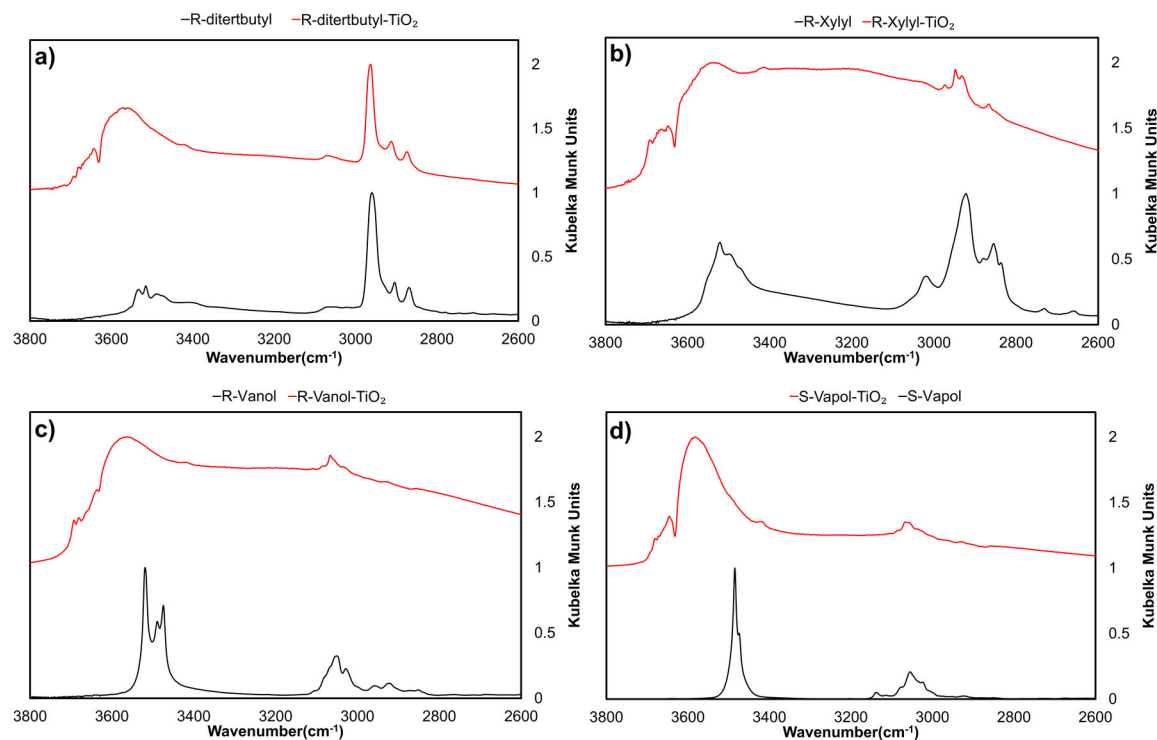


Figure S5. Normalized DRIFT spectra of BINOLates and grafted BINOLates (BINOLate-TiO₂) from 2600 to 3800 cm⁻¹ a) R-6,6'-di-tertbutyl-BINOL b) R-3,3'-xylyl-BINOL, c) R-VANOL, d) S-VAPOL. Spectra are stacked and normalized by their largest intensity for ease of comparison.

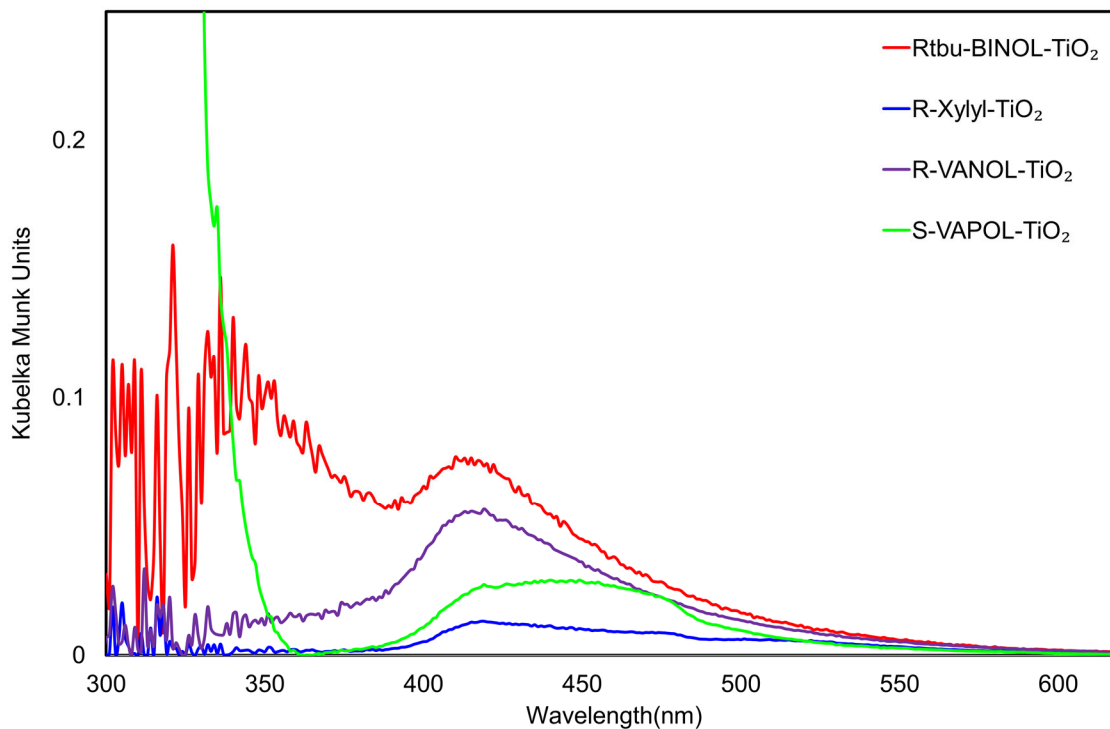


Figure S6. DRUV spectra of supported BINOLate-TiO₂ species. Spectra normalized by unmodified TiO₂ powder

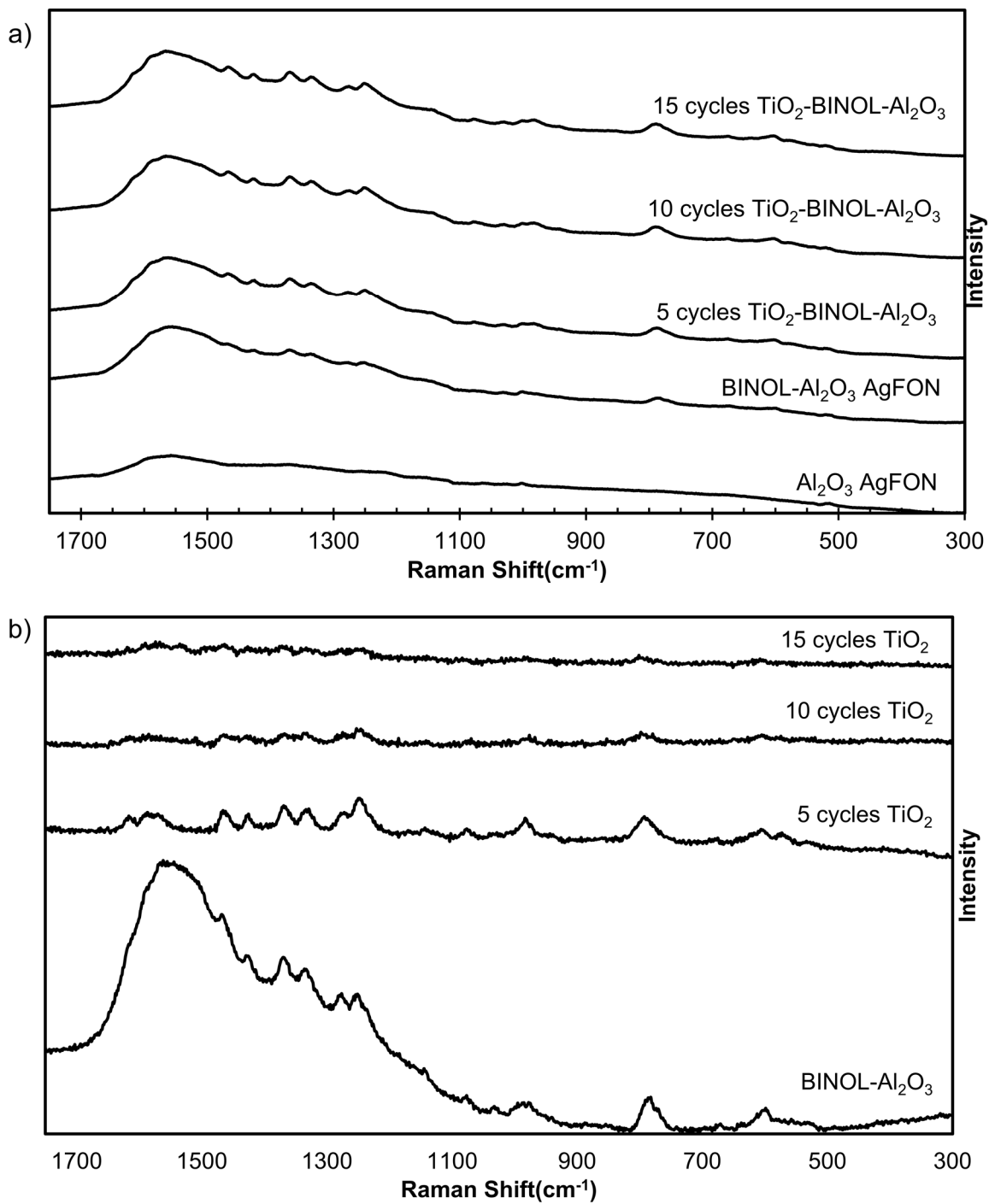


Figure S7. Surface enhanced Raman a) raw spectra, and b) and subtraction spectra of BINOL- Al_2O_3 modified by by 5, 10, and 15 cycles of Al_2O_3 by ALD. Subtracted spectra are the result of subtracting the raw spectra of one sample by the previous spectra.

Table S2. Observed SERS frequencies (ν , in cm^{-1}) of TiO_2 deposited on BINOL- Al_2O_3 -AgFON for 5, 10, and 15 cycles of TiO_2

BINOL- Al_2O_3 - AgFON	5c TiO_2 BINOL- Al_2O_3 - AgFON	10c TiO_2 - BINOL- Al_2O_3 - AgFON	15c TiO_2 - BINOL- Al_2O_3 - AgFON	Assignment
1614	1611	1611	1611	νCC , νCO , $\delta\text{O-H}$
1584	1584			νCC , δOH
	1570	1570	1570	νCO , νCC , νCC
1549			1533	-
1474			1485	νCC
	1463	1463	1466	νCC
1423	1423	1423	1423	νCC
1367	1367	1367	1367	νCO , νCC
1338	1331	1334	1327	-
1273	1273	1273		νCO , νCC , δCH
1248	1245	1245	1245	δCH
	1136			δCH
	1073	1072		νCC , δCCC , δCH
1032	1032			νCC , δCCC , δCH
1003	980	979	979	δCCC
788	791	791	791	γCH
771				νCC , γCH
	681			δCCC
	673			δCCC
666				τCC , γCH
594	604	603	601	τCC , γCH
	566			δCCC